ГЛАСНИК Српског географског друштва 105(2) 489-500
BULLETIN OF THE SERBIAN GEOGRAPHICAL SOCIETY 2025

Original scientific paper
UDC 551.242(594)
https://doi.org/10.2298/GSGD2502489A

Received: May 4, 2025
Corrected: July 21, 2025
Accepted: September 23, 2025

Ongky Anggara[1]*, Satrio Muhammad Alif*, Elysabet Sitinjak*, Jelita Rizki Simarmata*

* *Geomatics Engineering, Institut Teknologi Sumatera, South Lampung, Indonesia*

PRELIMINARY ESTIMATION SLIP RATE ALONG THE MANNA FAULT IN SUMATRAN FAULT ZONE, INDONESIA USING ALOS PALSAR 1 INSAR DATA

Abstract: The Sumatran Fault Zone (SFZ), Indonesia is a tectonically active region characterized by frequent seismic activity and significant geological features. In this study, we conducted a preliminary analysis using the Interferometric Synthetic Aperture Radar (InSAR) to asses the slip rate on the Manna Fault in the Sumatran Fault Zone (SFZ). We used ALOS PALSAR 1 satellite imagery to obtain information on deformation from the period 2007 to 2011 using the Small Baseline Subset (SBAS) method. Fault parallel velocities estimation from InSAR show the typical right-lateral slip of the Manna Fault. The slip rate of the Manna Fault estimated from this study is 8.6 mm/year. This study shows the potential of using InSAR with ALOS PALSAR I in monitoring slip rate in the Sumatra region. The InSAR technology can improve our understanding of seismic activity and potential earthquake hazards in the south Sumatra.

Keywords: tectonic deformation, SBAS InSAR, Manna Fault, surface displacement

Introduction

Sumatra Island is located in the Sumatran fault Zone (SFZ) which stretches 1900 km and is divided into 19 major fault Faults (Sieh & Natawidjaja, 2000). The Sumatran Fault represents a major dextral strike-slip fault zone which has the potential for earthquake hazard along the active fault line (Natawidjaja, 2018). Based on the history of earthquakes in the Sumatran Fault Zone, several significant events have been recorded over the past century. One notable earthquake occurred along the Kumering Fault on 24 June 1933, known as the

[1] ongky.anggara@gt.itera.ac.id (corresponding author)
Ongky Anggara (https://orcid.org/0009-0003-0020-1005)
Satrio Muhammad Alif (https://orcid.org/0000-0002-2923-3444)
Elysabet Sitinjak (https://orcid.org/0000-0003-0432-0231)

Liwa Earthquake (Mw 7.5), which caused severe damage in the Lake Ranau area (Hurukawa et al., 2014). Another major event was the earthquake along the Manna Fault in the highlands of Benkoelen, southern Sumatra, on 12 June 1893, with a magnitude of Mw 7.0, which also had a considerable impact on the surrounding region (Hurukawa et al., 2014). On February 15, 1994, the Liwa earthquake occurred with a magnitude of M 6.8 and caused severe damage to the surrounding area (Duquesnoy et al., 1996; Widiwijayanti et al., 1996). The Liwa area has the potential for significant potential hazards in the future (Triyoso & Suwondo, 2023). The last recorded earthquake along the Manna segment occurred in 1893, with a magnitude of Mw 7.0. This segment remains active and is considered to have the potential to generate future earthquakes.

The Manna Fault stretches for 196 km with a maximum credible magnitude of M 7.8 (Burton & Hall, 2014). The primary estimate of the slip rate of the Sumatran Fault systematically increases from south to north (Genrich et al., 2000; Prawirodirdjo et al., 2000), However, geological studies suggest that the average slip rate along the Sumatran Fault Zone is approximately 15–16 mm/year (Bradley et al., 2017; Natawidjaja, 2018). The GNSS data suggests that the overall present-day slip rates of the Sumatran Fault in Semangko Fault is 16.5 ± 2 mm/yr (Alif et al., 2020) and Kumering Fault is 18.2 ± 10 mm/yr (Alif et al., 2022). Geodetic data are needed to estimate the deformation along the Manna Fault and improve our understanding of its tectonic activity.

Many studies have calculated the slip rate of the Sumatran Fault using geological and geodetic methods (Alif et al., 2020; Bradley et al., 2017; Genrich et al., 2000; Ito et al., 2012; Meilano et al., 2012; Meilano et al., 2021; Alif et al., 2022; Natawidjaja, 2018; Sieh & Natawidjaja, 2000). However, slip rate estimation for the Manna Fault is limited due to the region's lack of detailed geodetic observations and geological investigations. This limitation highlights the need to estimate crustal deformation rates in the region to better understand its tectonic dynamics, especially considering that this segment still possesses significant earthquake potential, such as in the East Anatolia Fault Zone (EAFZ) with Mw 7.7 earthquake also exhibited left-lateral strike-slip characteristics (Liu et al., 2024). Slip rate estimation is very important for understanding the seismic potential of a region, as a basis for disaster mitigation planning, and for regional tectonic deformation modeling.

The deformation determination method can use GNSS (Alif et al., 2021; Anggara et al., 2025) and Interferometry Synthetic Aperture Radar (InSAR) (Elliott et al., 2008), such as volcanic activity (Anggara et al., 2023; Natadikara et al., 2023) and tectonic activity (Chlieh et al., 2008; Prawirodirdjo et al., 2010). The InSAR method is used to measure interseismic surface deformation (Liu et al., 2011), especially in Manna fault there is not sufficient distribution of GNSS observation points. The slip rate estimation using InSAR has been proven as a powerful tool in determining slip rate, such as in the Altyn Tagh Fault, northern Tibet (Elliott et al., 2008), The Ganzi-Yushu-Xianshuihe fault (Zhang et al., 2022), the Gyaring Co fault (GCF) in the central Tibetan Plateau (Zhang et al., 2023), the Garze–Yushu fault belt in the Tibetan Plateau (Liu et al., 2011), and Sumatran Fault (Tong et al., 2018). Interferometric Synthetic Aperture Radar (InSAR) can be used to measure crustal deformation, with an ablility to penetrate clouds, and an accuracy of millimeters per year (Elliott et al., 2016; Song et al., 2019). Permanent GNSS stations around the Manna Fault are still very rare, the available geodetic data is not sufficient for accurate estimation of crustal deformation rates. Due to the limitations of geodetic data, this study uses InSAR data as a slip rate analysis. The use of ALOS PALSAR-1 data fill the gap in geodetic observations in the

Manna Fault area and provide an initial estimate of its slip rate. This study uses ALOS PALSAR-1 images from 2007 to 2011. The use of ALOS PALSAR is based on the that Sumatra Island is covered by tropical rainforest, where temporal decorrelation poses a challenge for InSAR, L-band observations (such as ALOS PALSAR-1) are more effective in capturing ground deformation in densely vegetated areas (Tong et al., 2018). We processed the data using the Small Baseline Subset (SBAS) method to estimate time series of surface deformation for the Manna segment, then applied velocity corrections based on continuous GNSS observations. The corrected time series were used to calculate the fault slip rate, resulting in a more accurate and reliable estimate. This research uses ALOS PALSAR 1 images is preliminary to estimate the slip rate in the Manna Fault to provide an overview of estimates from InSAR. This research provides further insight into fault deformation activity in the Manna segment and its contribution to the potential for future earthquakes.

Materials and Methods

This study estimates slip rates in the Manna Fault located in southern Sumatra which are shown in Figure 1. We obtained 13 ALOS PALSAR 1 images with an observation period of 2007 to 2011, L-band specifications with ascending, as shown in Table 1. Data collection from 2007 to 2011 were obtained from https://search.asf.alaska.edu (accessed on 1 February 2023) the ALOS PALSAR I images. We performed a time series analysis using continuous GNSS velocity data from the CBKL station, provided by the Indonesian Geospatial Information Agency (BIG), to improve the InSAR time series.

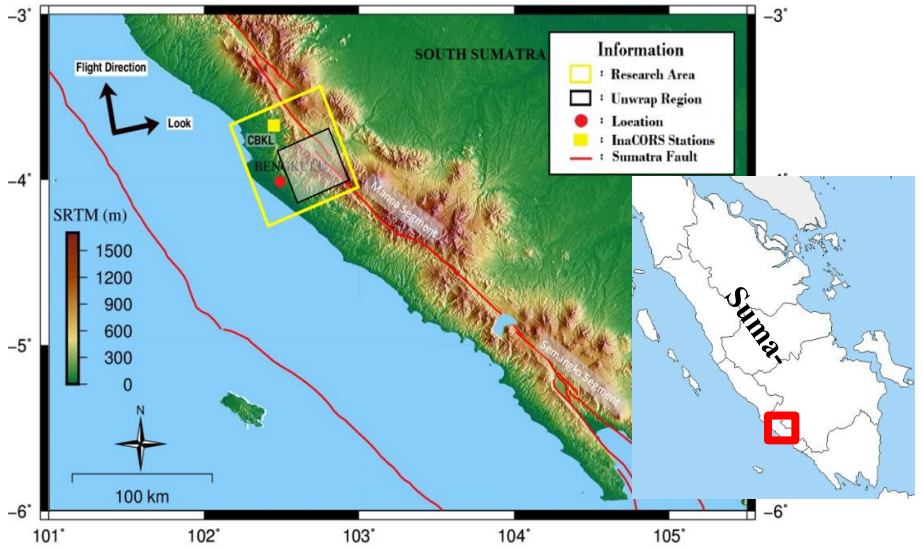

Fig. 1. Research area in the Sumatran Fault Zone (Manna Fault). The red lines represent the Sumatran Fault Zone (SFZ) and the Mentawai Fault (PuSGeN, 2017)

Table 1. Data Alos Palsar 1 Acquisition Details

No	**Image**	Acquisition Time
1	ALPSRP118677100-H1.0A	16/04/2008
2	ALPSRP098547100-H1.0A	30/11/2007
3	ALPSRP199197100-H1.0A	20/10/2009
4	ALPSRP259587100-H1.0A	08/12/2010
5	ALPSRP252877100-H1.0A	23/10/2010
6	ALPSRP246167100-H1.0A	07/09/2010
7	ALPSRP239457100-H1.0A	23/07/2010
8	ALPSRP219327100-H1.0A	07/03/2010
9	ALPSRP212617100-H1.0A	20/01/2010
10	ALPSRP192487100-H1.0A	04/09/2009
11	ALPSRP185777100-H1.0A	20/07/2009
12	ALPSRP165647100-H1.0A	04/03/2009
13	ALPSRP145517100-H1.0A	17/10/2008

Then, we use GNSS data provided by the Geospatial Information Agency (BIG) (CBKL stations). GNSS data are processed using BERNESE 5.2 to obtain daily solutions of GNSS sites (Dach et al., 2015). The reference sites refer to the International GNSS Service (IGS) sites (e.g., Alif et al., 2025), in the International Terrestrial Reference System (ITRF) 2014 (Altamimi et al., 2016), then the velocity was calculated by linear regression. We conducted the analysis using the Small Baseline Subset (SBAS) technique to extract time-series ground deformation from the InSAR data (e.g., Orhan, 2021), to analyze interseismic deformation in the Manna Fault. In this study, we performed time-series InSAR analysis using the Small Baseline Subset (SBAS) method (e.g., Anggara et al., 2025). The processing was conducted using the open-source software GMTSAR (Sandwell et al., 2010) to generate interferogram images. Shuttle Radar Topography Mission (SRTM) with a 30 m resolution dataset is used to remove the topographic phase (Farr et al., 2007), and all differential interferograms are unwrapped using the Statistical-cost network-flow method for phase unwrapping (SNAPHU) (Chen & Zebker, 2002).

The SBAS algorithm is a robust InSAR time series analytical approach that uses interferograms with small baselines to minimize spatial decoration effects and topographic errors (Lingyun et al., 2013; Qu et al., 2022). Then, GNSS velocity was converted from 3D (Easting. Northing, Up) to 1D Line of Sight (LOS) to correct the LOS InSAR results, respectively (e.g., Struhár et al., 2022). To compare GNSS velocities with InSAR measurements, the horizontal GNSS observations were converted into Line-of-Sight (LOS) deformation using the local incidence and azimuth angles (Zhu et al., 2021), then the calculate decomposition fault-parallel (Dong et al., 2020; Song et al., 2019; Zhu et al., 2021). We model the fault slip rates using a screw dislocation model (Qiu et al., 2019; Savage & Burford, 1973) which is defined equation below:

$$S=\frac{V}{\pi}\tan^{-1}\frac{x}{D} \quad (1)$$

Where S is the fault parallel velocity InSAR, V is slip rate, D is fixed to 30 km, x is distance from the fault. The slip rates is ranging from 0 mm/yr to 30 mm/yr with an interval of 0.2 mm/yr. Then we find the best values that minimum ($\chi 2$) the misfit between the calculated profile by the model and the observed profile by InSAR observation.

Results and Discussion

ALOS PALSAR 1 using the larger L-band band wavelength (approximately 23.5 cm), which is in areas with high vegetation affects the results of coherence and co-registration (Alif et al., 2023; Grzovic & Ghulam, 2015). In our study, we mitigated this by reducing these effects through processing (coregistration and atmospheric filtering) to produce a good interferogram time series. We then obtained multi-temporal data by using least squares inversion to estimate a constant rate on each pixel (Biggs et al., 2007; Zhu et al., 2021). The LOS results show that the satellite visibility is getting further away or closer from the ascending direction. Data acquisition was carried out on an ascending track, where the satellite moves northward and observes eastward. In this configuration, positive line-of-sight deformation values indicate motion toward the satellite, which can correspond to eastward horizontal displacement or vertical uplift. respectively, negative values indicate motion away from the satellite, reflecting westward displacement or vertical subsidence. Line of Sight (LOS) displacement results from the ALOS PALSAR 1 image show that the interseismic rate map value in the Manna Fault area is relatively large with a maximum LOS value of 2314.83 mm/yr and a minimum value of 308.27 mm/yr shown in Figure 2. Line of sight (LOS) displacement results, the empty LOS value has been corrected by considering coherence data, where low coherence values are generally caused by high vegetation cover which results in temporal decorrelation (Alif et al., 2023).

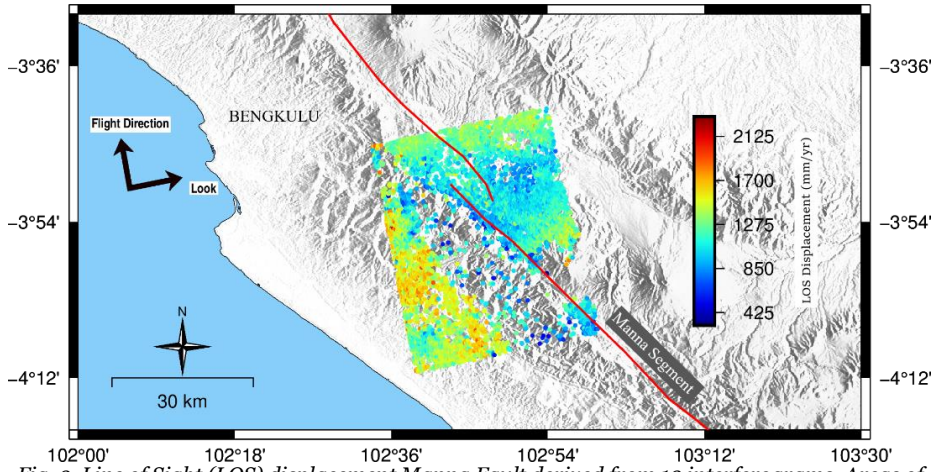

Fig. 2. Line of Sight (LOS) displacement Manna Fault derived from 13 interferograms. Areas of movement away from the satellite are shown by positive values (red), and areas of movement toward the satellite are represented by blue values

The parallel fault results are calculated based on the Line of Sight (LOS) displacement value in the ascending direction. The fault-parallel velocity component was calculated from ALOS PALSAR-1 InSAR data by projecting the line of sight (LOS) displacement velocity to the local strike direction of the Sumatra Fault Zone (SFZ) in the Manna segment. The fault parallel projection results show velocity values ranging from 0 mm/year to 480 mm/year, indicating significant differential movement along the Manna segment (Figure 3). The estimation assuming only horizontal motion with each LOS velocity observation is converted to a fault-parallel velocity by considering the incidence angle for the pixel measured (Garthwaite et al., 2013). Fault parallel results show the Manna Fault on the western side of the

SFZ is directed northwestward and on the eastern part of the SFZ is directed southwestward. The deformation distribution pattern shows the typical characteristics of strike-slip deformation in the SFZ. The highest values are concentrated around the main fault line, indicating a zone of stress accumulation (Rafie et al., 2023).

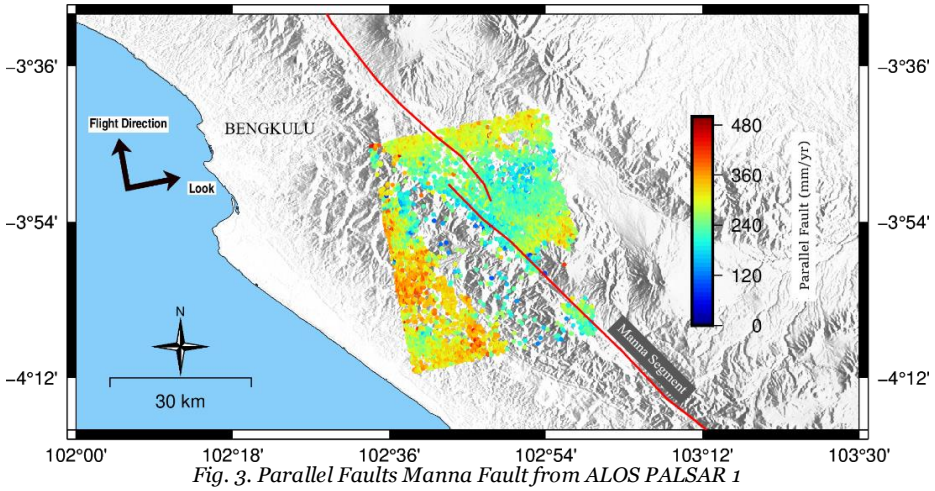

Fig. 3. Parallel Faults Manna Fault from ALOS PALSAR 1

The fault parallel results are corrected for LOS velocity, we combine continuous GNSS station data near the Manna segment. The GNSS-corrected velocity field is used to calibrate the LOS results from the fault parallel to reduce possible atmospheric bias and improve the reliability of the slip rate estimates. The Parallel Fault results were corrected using the velocity of the GNSS station, in the Manna Fault using the CBKL station. Correction LOS velocity with GNSS velocity data can improve the spatial resolution (Wang et al., 2019). The results show that the fault-parallel value for the Manna Fault is ~0 mm/yr to ~24 mm/yr (Figure 4). This corrected range shows more reliable slip rate estimates, consistent with previous geodetic observations along other segments of the Sumatran Fault Zone.

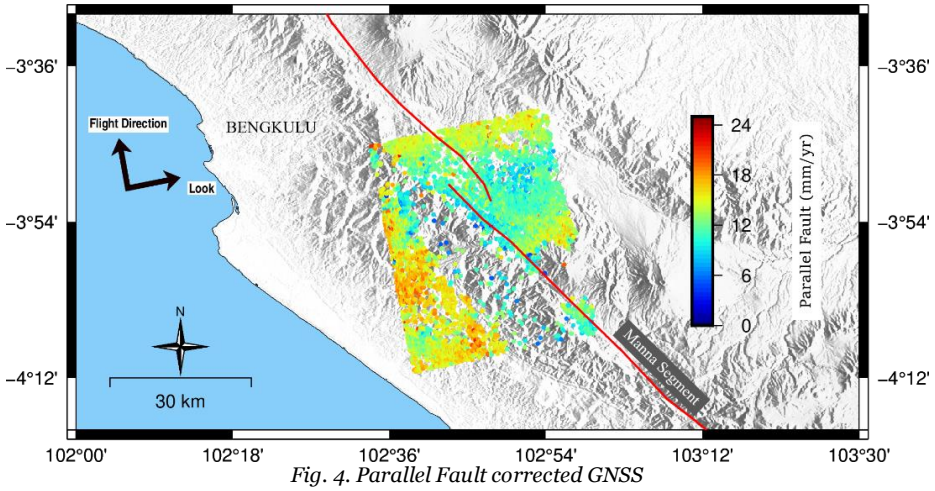

Fig. 4. Parallel Fault corrected GNSS

In the preliminary study, in Toba (2.2° N) based on GNSS velocity indicated a slip rate of ~30 mm/yr (Prawirodirdjo et al., 2000), the results were similar to the approach using campaign GNSS with slip rates (0.8°S to 2.7°N) of 22 to 26 mm/yr (Genrich et al., 2000). The slip rate in Aceh is 4.0°N to 5.5°N with an estimated slip deficit rate of 20 mm/year (Ito et al., 2012). These results indicate a consistent increase from southward to northward (Mccaffrey, 1992; Sieh & Natawidjaja, 2000). However, the obliquity of underthrusting beneath the forearc, this velocity component is sensitive to both the strike-slip fault and the frictionally related Sunda megathrust (Bradley et al., 2017). According to the most present-day estimations, the value of slip rates has not consistently increased as estimated previously (Alif et al., 2020; Bradley et al., 2017; Meilano, 2021; Alif et al., 2022; Natawidjaja, 2018). The estimation GNSS slip rates from previous estimates in nearly with Manna Fault such as, the Semangko Faults is 16.5 ± 2 mm/yr (Alif et al., 2020) and 14±3 mm/yr (Meilano et al., 2021) and the Kumering Fault is 18.2 ± 10 mm/year (Alif et al., 2022). This study estimation of the slip rate derived from InSAR data results shows that the Manna Fault is 8.60 mm/yr with a minimum $\chi 2$ value of 2.25 (Figure 5). In the Manna Fault, the estimate is preliminary with the slip rate value using InSAR which still needs to be elaborated with geological slip rate results or estimates using GNSS slip rate. However, in the Manna Fault, earthquakes occur with a maximum credible of M 7.8 (Burton & Hall, 2014), The magnitude of the earthquake is obtained from relation rupture, length, and magnitude (Wells & Coppersmith, 1994). The estimated potential for earthquake energy accumulation with a Manna Fault with a rupture length of 85 km with a 100-year return period of Mw 7.2 and a 200-year return period of Mw 7.4 (Natawidjaja, 2007), which has a high earthquake potential in the Manna Fault in the future. These findings support the interpretation that the Manna segment is actively undergoing interseismic deformation and indicate a tectonic potential that has not been widely observed before.

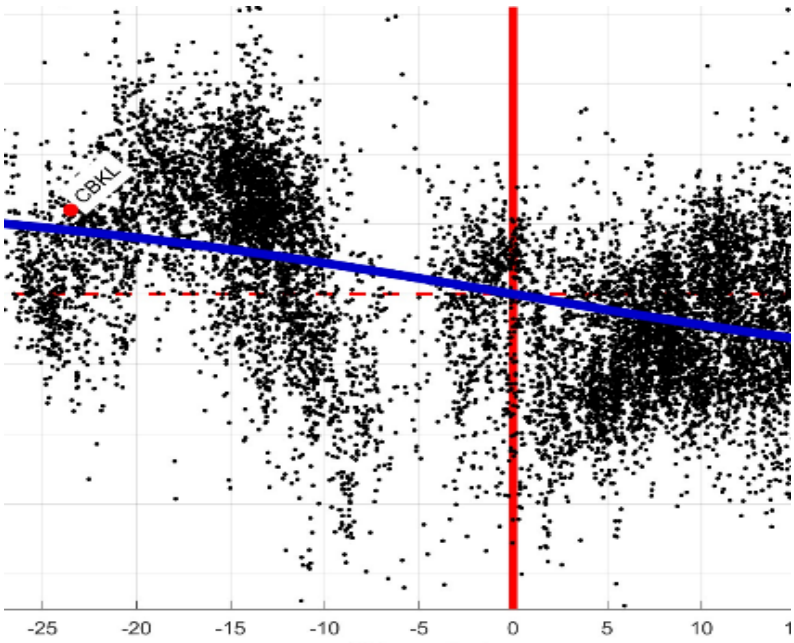

Fig. 5. The model sliprate of Manna Fault. Black points are fault parallel velocities. The red thick line shows Manna Fault. Red point show the fault parallel velocities derived from GNSS. Blue line is the slip rate of Manna Fault

Conclusion

In this study, the slip rate analysis of the Manna Fault in the Sumatra region was conducted using ALOS PALSAR I images. The results of our preliminary analysis provide valuable insights into the slip rates of these faults. Our findings reveal that the slip rate along the Manna Fault is estimated at approximately 8.60 mm/yr, with a corresponding minimum $\chi 2$ value of 2.25. These findings provide a preliminary understanding of the fault activity in the region. It is important that the slip rate estimate for the Manna Fault presented in this study is preliminary and would improve the estimation through further validation and elaboration through geological slip rate and geodetic slip rate.

Acknowledgments: The authors thank the the Japanese Aerospace and Exploration Agency (JAXA) for providing data used in this research and the Indonesian Geospatial Information Agency (BIG) for providing GNSS continuous. The map was created using Generic Mapping Tools (GMT) software (Wessel et al., 2013).

Conflicts of Interest: The authors declare no conflict of interest.

Publisher's Note: Serbian Geographical Society stays neutral with regard to jurisdictional claims in published maps and institutional affiliations.

References

Alif, S. M., Anggara, O., Ristiana, V., & Engineering, G. (2023). Coherence analysis of Sentinel-1A images in various land. *Jurnal Geografi Gea, 23*(2), 135–143. https://doi.org/10.17509/gea.v23i2.61258

Alif, S. M., Cahyani, P. F., Anggara, O., & Rizqiansyah, A. (2022). Slip rate of Kumering Fault in Lampung Province calculated from GPS data (2007–2021). *Jurnal Geosains dan Teknologi, 5*(2), 83–90. https://doi.org/10.14710/jgt.5.2.2022.83-90

Alif, S. M., Fattah, E. I., & Kholil, M. (2020). Geodetic slip rate and locking depth of East Semangko Fault derived from GPS measurement. *Geodesy and Geodynamics, 11*(3), 222–228. https://doi.org/10.1016/j.geog.2020.04.002

Alif, S. M., Fattah, E. I., Kholil, M., & Anggara, O. (2021). Source of the 2019 Mw 6.9 Banten intraslab earthquake modelled with GPS data inversion. *Geodesy and Geodynamics, 12*(4), 308–314. https://doi.org/10.1016/j.geog.2021.06.001

Alif, S., Erlando, M., Anggara, O., & Nurhayati, M. (2025). Impact of baseline length on uncertainty in static relative GNSS positioning. *Journal of Applied Geodesy*, *19*(4), 575-583. https://doi.org/10.1515/jag-2024-0090

Altamimi, Z., Rebischung, P., Métivier, L., & Collilieux, X. (2016). ITRF2014: A new release of the International Terrestrial Reference Frame modeling nonlinear station motions. *Journal of Geophysical Research: Solid Earth, 121*(8), 6109–6131. https://doi.org/10.1002/2016JB013098

Anggara, O., Meilano, I., Alif, S. M., Susilo, S., & Setyadji, A. B. (2025). Present-day crustal deformation in central Sumatra, Indonesia derived from GNSS observation and tectonic implications. *Geodesy and Geodynamics*. https://doi.org/10.1016/j.geog.2025.05.002

Anggara, O., Welly, T. K., Fauzi, A. I., Alif, S. M., Perdana, R. S., Oktarina, S. W., Nuha, M. U., & Rosadi, U. (2023). Monitoring ground deformation of Sinabung volcano eruption (2018–2019) using DInSAR technique and GPS data. *AIP Conference Proceedings*, 2654. https://doi.org/10.1063/5.0114428

Anggara, O., Sonya, P., Perdana, R. S., Pangestika, D. M., Try Atmojo, A., Galih Suhadha, A., Alif, S. M., & Perdana, A. M. P. (2024, September). Recent analysis of land subsidence rates in Medan, Indonesia, using time-series InSAR (2015–2023). *In International Seminar on Aerospace Science and Technology* (pp. 55–65). Springer Nature Singapore. https://doi.org/10.1007/978-981-96-1344-1_6

Biggs, J., Wright, T., Lu, Z., & Parsons, B. (2007). Multi-interferogram method for measuring interseismic deformation: Denali Fault, Alaska. *Geophysical Journal International, 170*(3), 1165–1179. https://doi.org/10.1111/j.1365-246X.2007.03415.x

Bradley, K. E., Feng, L., Hill, E. M., Natawidjaja, D. H., & Sieh, K. (2017). Implications of diffuse deformation of the Indian Ocean lithosphere for slip partitioning in Sumatra. *Journal of Geophysical Research: Solid Earth, 122*(1), 572–591. https://doi.org/10.1002/2016JB013549

Burton, P. W., & Hall, T. R. (2014). Segmentation of the Sumatran fault. *Geophysical Research Letters, 41*(12), 4149–4158. https://doi.org/10.1002/2014GL060242

Chen, C. W., & Zebker, H. A. (2002). Phase unwrapping for large SAR interferograms: Statistical segmentation and generalized network models. *IEEE Transactions on Geoscience and Remote Sensing, 40*(8), 1709–1719. https://doi.org/10.1109/TGRS.2002.802453

Chlieh, M., Avouac, J. P., Sieh, K., Natawidjaja, D. H., & Galetzka, J. (2008). Heterogeneous coupling of the Sumatran megathrust. *Journal of Geophysical Research: Solid Earth, 113*(5), 1–31. https://doi.org/10.1029/2007JB004981

Dach, R., Andritsch, F., Arnold, D., Bertone, S., Fridez, P., Jäggi, A., Jean, Y., Lutz, S., Maier, A., Mervart, L., Meyer, U., Orliac, E., Prange, L., Schaer, S., Sidorov, D., Susnik, A., Villiger, A., Walser, P., & Thaller, D. (2015). Bernese GNSS Software Version 5.2. Astronomical Institute, University of Bern. https://doi.org/10.7892/boris.72297

Dong, Y., Meng, G., & Hong, S. (2020). Coseismic and postseismic deformation of the 2016 Mw 6.6 Aketao earthquake from InSAR observations and modeling. *Pure and Applied Geophysics, 177*(1), 265–283. https://doi.org/10.1007/s00024-019-02092-9

Duquesnoy, T., Bellier, O., Kasser, M., Sébrier, M., Vigny, C., & Bahar, I. (1996). Deformation related to the 1994 Liwa earthquake. *Geophysical Research Letters, 23*(21), 3055–3058. https://doi.org/10.1029/96GL02818

Elliott, J. R., Biggs, J., Parsons, B., & Wright, T. J. (2008). InSAR slip rate determination on the Altyn Tagh Fault. *Geophysical Research Letters, 35*(12), 1–5. https://doi.org/10.1029/2008GL033659

Elliott, J. R., Walters, R. J., & Wright, T. J. (2016). Space-based observation in understanding earthquakes. *Nature Communications, 7*, 1–16. https://doi.org/10.1038/ncomms13844

Farr, T. G., Rosen, P. A., Caro, E., Crippen, R., Duren, R., Hensley, S., Kobrick, M., Paller, M., Rodriguez, E., Roth, L., Seal, D., Shaffer, S., Shimada, J., Umland, J., Werner, M.,

Oskin, M., Burbank, D., & Alsdorf, D. (2007). The Need for Global Topography. *Reviews of Geophysics, 45*(2), 1–43. http://www2.jpl.nasa.gov/srtm/SRTM_paper.pdf

Garthwaite, M. C., Wang, H., & Wright, T. J. (2013). Broadscale interseismic deformation and fault slip rates in the central Tibetan Plateau observed using InSAR. *Journal of Geophysical Research: Solid Earth, 118*(9), 5071–5083. https://doi.org/10.1002/jgrb.50348

Genrich, J. F., Bock, Y., McCaffrey, R., Prawirodirdjo, L., Stevens, C. W., Puntodewo, S. S. O., Subarya, C., & Wdowinski, S. (2000). Distribution of slip at the northern Sumatran fault system. *Journal of Geophysical Research: Solid Earth, 105*(B12), 28327–28341. https://doi.org/10.1029/2000jb900158

Grzovic, M., & Ghulam, A. (2015). Evaluation of land subsidence from underground coal mining using TimeSAR (SBAS and PSI) in Springfield, Illinois, USA. *Natural Hazards, 79*(3), 1739–1751. https://doi.org/10.1007/s11069-015-1927-z

Hurukawa, N., Wulandari, B. R., & Kasahara, M. (2014). Earthquake history of the Sumatran fault, Indonesia, since 1892, derived from relocation of large earthquakes. *Bulletin of the Seismological Society of America, 104*(4), 1750–1762. https://doi.org/10.1785/0120130201

Ito, T., Gunawan, E., Kimata, F., Tabei, T., Simons, M., Meilano, I., Agustan, A., Ohta, Y., Nurdin, I., & Sugiyanto, D. (2012). Isolating along-strike variations in the depth extent of shallow creep and fault locking on the northern Great Sumatran Fault. *Journal of Geophysical Research (Solid Earth), 117*, Article 6409. https://doi.org/10.1029/2011JB008940

Lingyun, J., Qingliang, W., & Shanlan, Q. (2013). Present-day deformation of Agung volcano, Indonesia, as determined using SBAS-InSAR. *Geodesy and Geodynamics, 4*(3), 65–70. https://doi.org/10.3724/sp.j.1246.2013.03065

Liu, Y., Xu, C., Li, Z., Wen, Y., & Forrest, D. (2011). Interseismic slip rate of the Garze-Yushu fault belt in the Tibetan Plateau from C-band InSAR observations between 2003 and 2010. *Advances in Space Research, 48*(12), 2005–2015. https://doi.org/10.1016/j.asr.2011.08.020

Liu, J., Huang, C., Zhang, G., Shan, X., Korzhenkov, A., & Taymaz, T. (2024). Immature characteristics of the East Anatolian Fault Zone from SAR, GNSS and strong motion data of the 2023 Türkiye–Syria earthquake doublet. *Scientific Reports, 14*, Article 10625. https://doi.org/10.1038/s41598-024-61326-6

McCaffrey, R. (1992). Oblique plate convergence, slip vectors, and forearc deformation. *Journal of Geophysical Research, 97*(B6), 8905–8915. https://doi.org/10.1029/92JB00483

Meilano, I., Abidin, H. Z., Andreas, H., Gumilar, I., Sarsito, D., Rahma, H., Rino, Harjono, H., Kato, T., Kimata, F., & Fukuda, Y. (2012). Slip rate estimation of the Lembang Fault, West Java, from geodetic observation. *Journal of Disaster Research, 7*(1), 12–18. https://doi.org/10.20965/jdr.2012.p0012

Meilano, I., Salman, R., Rahmadani, S., Shi, Q., Susilo, S., Lindsey, E., Supendi, P., & Daryono, D. (2021). Source characteristics of the 2019 Mw 6.5 Ambon, Eastern Indonesia, earthquake inferred from seismic and geodetic data. *Seismological Research Letters, 92*(6), 3339–3348. https://doi.org/10.1785/0220210021

Meilano, I., Susilo, S., Gunawan, E., & Parjanto, B. (2021). Geodetic slip rate estimates for the Kumering and Semangko segments of the Sumatera Fault. *Jurnal Meteorologi dan Geofisika, 22*, Article 39. https://doi.org/10.31172/jmg.v22i1.802

Meilano, I., Susilo, S., Gunawan, E., & Rahmadani, S. (2021). Coseismic and postseismic deformation from the 2007 Bengkulu earthquake based on GPS data. *RISET Geologi dan Pertambangan, 31*(2), 98. https://doi.org/10.14203/risetgeotam2021.v31.1182

Natadikara, R., Fauzi, A. I., Anggara, O., Perdana, R. S., Alif, S. M., Julzarika, A., Nurtyawan, R., & Rohman, A. (2023). Monitoring deformation of Anak Krakatoa volcano using differential InSAR. *AIP Conference Proceedings, 2941*(1). https://doi.org/10.1063/5.0181540

Natawidjaja, D. H. (2007). The Sumatran fault zone—from source to hazard. *Journal of Earthquake and Tsunami, 1*, 21–47.

Natawidjaja, D. H. (2018). Updating active fault maps and slip rates along the Sumatran Fault Zone, Indonesia. *IOP Conference Series: Earth and Environmental Science, 118*(1). https://doi.org/10.1088/1755-1315/118/1/012001

Orhan, O. (2021). Monitoring of land subsidence due to excessive groundwater extraction using small baseline subset technique in Konya, Turkey. *Environmental Monitoring and Assessment, 193*(4), Article 10661. https://doi.org/10.1007/s10661-021-08962-x

Prawirodirdjo, L., Bock, Y., Genrich, J. F., Puntodewo, S. S. O., Rais, J., Subarya, C., & Sutisna, S. (2000). One century of tectonic deformation along the Sumatran fault from triangulation and GPS surveys. *Journal of Geophysical Research: Solid Earth, 105*(B12), 28343–28361. https://doi.org/10.1029/2000JB900150

Prawirodirdjo, L., McCaffrey, R., Chadwell, C. D., Bock, Y., & Subarya, C. (2010). Geodetic observations of an earthquake cycle at the Sumatra subduction zone: Role of interseismic strain segmentation. *Journal of Geophysical Research: Solid Earth, 115*(B03410). https://doi.org/10.1029/2008JB006139

PuSGeN (2017). *Peta sumber dan bahaya gempa Indonesia tahun 2017*. Kementerian PUPR.

Qiu, J., Liu, L., Wang, C., & Wang, Y. (2019). Present-day tectonic activity along the central section of the Altyn Tagh fault derived from time series InSAR. *Geodesy and Geodynamics, 10*(4), 307–314. https://doi.org/10.1016/j.geog.2019.03.008

Qu, F., Zhang, Q., Niu, Y., Lu, Z., Wang, S., Zhao, C., Zhu, W., Qu, W., & Yang, C. (2022). Mapping vertical crustal deformation of the Weihe Basin using Sentinel-1 and ALOS-2. *Remote Sensing, 14*(13), 1–21. https://doi.org/10.3390/rs14133182

Rafie, M. T., Sahara, D. P., Cummins, P. R., Triyoso, W., & Widiyantoro, S. (2023). Stress accumulation and earthquake activity on the Great Sumatran Fault, Indonesia. Natural Hazards, 116(3), 3401–3425. https://doi.org/10.1007/s11069-023-05816-2 Sandwell, D., Mellors, R., Tong, X., Xu, X., Wei, M., & Wessel, P. (2010). *GMTSAR Software for Rapid Assessment of Earthquakes*. AGU Fall Meeting Abstracts.

Savage, J. C., Burford, R. O. (1973). Savage, J. C., and R. O. Burford. "Geodetic determination of relative plate motion in central California. *Journal of Geophysical Research, 78*(5), 832–845.

Sieh, K., & Natawidjaja, D. (2000). Neotectonics of the Sumatran fault, Indonesia. *Journal of Geophysical Research: Solid Earth, 105*(B12), 28295–28326. https://doi.org/10.1029/2000jb900120

Song, X., Jiang, Y., Shan, X., Gong, W., & Qu, C. (2019). A fine velocity and strain rate field of present-day crustal motion of the northeastern Tibetan Plateau inverted jointly by InSAR and GPS. *Remote Sensing, 11*(4). https://doi.org/10.3390/rs11040435

Tong, X., Sandwell, D. T., & Schmidt, D. A. (2018). Surface Creep Rate and Moment Accumulation Rate Along the Aceh Segment of the Sumatran Fault From L-band ALOS-

1/PALSAR-1 Observations. *Geophysical Research Letters, 45*(8), 3404–3412. https://doi.org/10.1002/2017GL076723

Triyoso, W., & Suwondo, A. (2023). From the geodynamic aspect to earthquake potential hazard analysis of Liwa city and its surrounding. *Natural Hazards, 116*(1), 1329–1344. https://doi.org/10.1007/s11069-022-05705-0

Wang, H., Wright, T. J., Liu-Zeng, J., & Peng, L. (2019). Strain Rate Distribution in South-Central Tibet from Two Decades of InSAR and GPS. *Geophysical Research Letters, 46*(10), 5170–5179. https://doi.org/10.1029/2019GL081916

Wells, D. L., & Coppersmith, K. J. (1994). New empirical relationships among magnitude, rupture length, rupture width, rupture area, and surface displacement. *Bulletin Seismological Society of America, 84*(4), 974–1002. https://doi.org/10.1785/BSSA0840040974

Wessel, P., Smith, W., Scharroo, R., Luis, J., & Wobbe, F. (2013). Generic Mapping Tools: Improved Version Released. *Eos Transactions American Geophysical Union, 94*. https://doi.org/10.1002/2013EO450001

Widiwijayanti, C., Déverchère, J., Louat, R., Sébrier, M., Harjono, H., Diament, M., & Hidayat, D. (1996). Aftershock sequence of the 1994, Mw 6.8, Liwa earthquake (Indonesia): Seismic rupture process in a volcanic arc. *Geophysical Research Letters, 23*(21), 3051–3054. https://doi.org/10.1029/96GL02048

Zhang, Q., Li, Y., Zhang, J., Tian, Y., Tian, T., & Li, B. (2023). Slip deformation along the Gyaring Co fault from InSAR and GPS. *Acta Geophysica, 71*(1), 53–63. https://doi.org/10.1007/s11600-022-00920-6

Zhang, W., Ji, L., Zhu, L., Liu, C., Jiang, F., & Xu, X. (2022). Current Slip and Strain Rate Distribution Along the Ganzi-Yushu-Xianshuihe Fault System Based on InSAR and GPS Observations. *Frontiers in Earth Science, 10*, 1–16. https://doi.org/10.3389/feart.2022.821761

Zhu, L., Ji, L., & Liu, C. (2021). Interseismic slip rate and locking along the Maqin–Maqu Segment of the East Kunlun Fault, Northern Tibetan Plateau, based on Sentinel-1 images. *Journal of Asian Earth Sciences, 211*, Article 104703. https://doi.org/10.1016/j.jseaes.2021.104703